INVESTIGATIONS ON LOW-COST AND EFFICIENT BI-LAYERED METAL OXIDE THIN FILM ELECTRODES FOR PHOTOELECTROCHEMICAL WATER SPLITTING

Synopsis

Submitted in the partial fulfilment for the requirement of

Doctor of Philosophy

In

Chemistry

Submitted by

KUMARI RUCHI

Under the supervision of

PROF. ROHIT SHRIVASTAV
Head, Department of Chemistry

Department of Chemistry, Faculty of Science

Dayalbagh Educational Institute (Deemed to be a university)

Dayalbagh, Agra-282005

2022

1. Introduction

One of the most important components required to support life on Earth is energy. It is also an important factor in a country's economic development. Fossil fuels (coal, oil, and natural gas) currently meet more than 90% of the world's energy requirements. Fossil fuels are non-renewable, and their generation takes thousands of years. Furthermore, there are serious environmental issues linked with the large-scale burning of fossil fuels, such as the generation of greenhouse gases (GHGs). Transportation, electricity generation, diesel generation, and other sources emit almost thirty billion tonnes of SO_2, CO_2, CO, and NO_x each year. Acid rain is caused by the exhaled GHGs, which harm lakes and forests [Dass S. et al, 2000]. It also contributes to global warming. The world is becoming increasingly complex. Global population growth has resulted in a nearly exponential increase in energy demand. It has compelled us to explore for more sustainable and renewable energy sources to replace finite fossil fuels. Because fossil fuels are likely to become scarce in the future, renewable alternatives such as wind, solar, hydro, and geothermal energy are being investigated.

In recent years, researchers all around the world have focused their attention on the utilisation of solar energy as one of several renewable energy sources. Solar energy is safe, easy to obtain, and represents a nearly limitless source of energy capable of meeting the entire world's energy requirements. It will not run out any time soon, unlike fossil fuels. Solar energy, on the other hand, is subject to the availability of sunshine on the earth's surface. Solar energy can be used for a variety of purposes, including the generation of electricity (through solar panels) and hydrogen (by water splitting). According to a study, solar and wind energy can produce 1110 billion kg of hydrogen. Hydrogen is seen as a possible replacement of liquid and fossil fuels as an energy carrier. Hydrogen has been widely identified as the fuel for the next generation, owing to its high enthalpy of combustion (286 kJ/mol), and is thought to have the capacity to meet the world's increasing energy need in the near future. H_2 has a calorific value of 141.8 kJ/g, which is three times more than gasoline. As a result, it is a desirable and environmentally friendly fuel, as it produces only water when burned. Hydrogen is one of the most abundant elements on Earth, with features such as low density, high thermal conductivity, nontoxic, non-metallic, odourless, tasteless, colourless, highly flammable, and strong reducing capabilities that make it ideal for use as an energy carrier. It also has large capability for storing

energy. It has a wide range of possible applications, including non-polluting vehicle power, household heating, and much more. As a result, hydrogen as a fuel is expected to join photovoltaic electricity as the core of a future sustainable energy system [Bak et al 2002].

Water splitting via photoelectrochemical (PEC) route is based on the notion of converting light energy into chemical energy. A PEC cell is a device that converts radiant energy into chemical energy. It typically consists of a semiconductor electrode (anode) and a platinum (Pt) counter electrode (cathode), both of which are immersed in aqueous electrolyte solution [Bak et al 2002]. In recent years, there has been a lot of interest in capturing solar energy and converting it to a directly useable chemical fuel, such as hydrogen, via PEC splitting of water. The phenomenon of PEC water splitting was first documented in 1972 [Fujishima et al 1972]. Irradiation causes electron-hole pairs to form on the semiconductor, which interact with the ionic species present in the solution at the solid/liquid interface. The hydrogen evolution reaction (HER) is driven by photogenerated electrons at the cathode, whereas the oxygen evolution reaction (OER) is driven by photogenerated holes at the anode surface. Because holes are the minority charge carriers in an n-type semiconductor, it is suitable for use as photoanode. A p-type semiconductor is suitable for use as photocathode because electrons are the minority charge carriers. The photoelectrode utilised must be capable of absorbing the greatest amount of solar energy, while also having a high catalytic function for water splitting. For electrochemical breakdown of water, the needed electromotive force (EMF) must be equal to or greater than 1.23 eV [Bak et al 2002]. However, due to overpotential losses at the anode and cathode, water breakdown does not occur exactly at 1.23 eV, and a higher operating voltage is required. As a result, the recombination rate of electron hole pairs created after light absorption in a PEC cell must be low for greater energy conversion efficiency. In order to absorb the most solar energy, the semiconductor must also have a matching band gap that is in tune with the solar spectrum.

The usage of thin nanostructured films of inorganic material has been the focus of study in this area so far (particularly metal oxides). Different researchers have looked at the usage of various dopants to improve the efficiency of these nanostructures. Various synthesis processes, such as electrodeposition, sol gel approach, spray pyrolysis, and atmospheric pressure chemical vapour deposition etc. can be used to tailor the morphology of these nanostructures for increased performance [Chiam et al 2014].

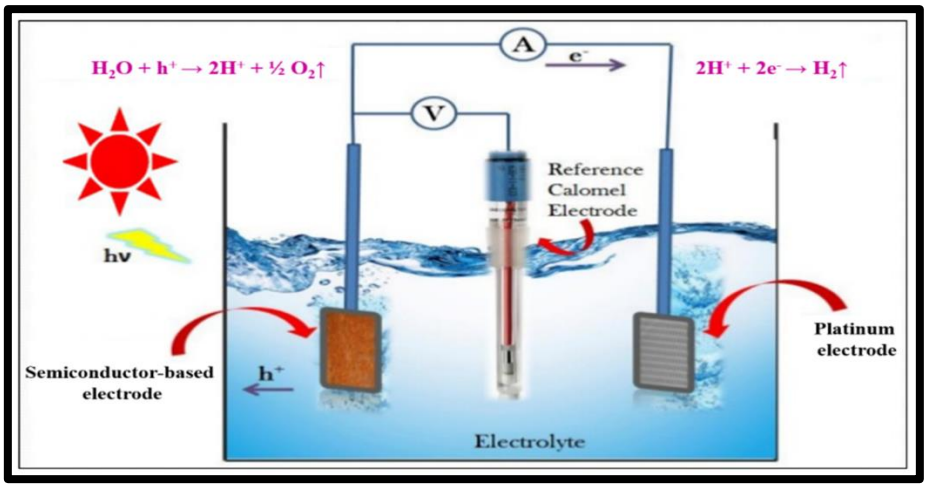

Fig. 1: Schematic of reaction pathway for Photoelectrochemical water splitting (Goettmann et al (2006))

2. Methods to enhance the PEC performance

Photoelectrodes investigated so far by different researchers suffer with one or more limitations, including low light absorption, poor charge separation, and low surface charge transfer efficiency. To overcome these limitations, extensive research is underway world over. Performance of photoelectrodes are being modulated by including sacrificial reagent addition, cocatalyst dispersion, cationic/anionic doping, heterojunction formation, metal loading, dye sensitization, non-metal doping, transitional metal incorporation, conjugated polymer modification, coupling with other semiconductors, introduction of carbon-dopants and anchoring carbonaceous materials, and so on. The fusing of two-conjugated material systems not only stabilises the hybrid, but also enhances solar spectral harnessing by extending optical absorption to a longer wavelength range. Combining with various carbon-rich materials not only compensates for the shortcomings of individual semiconductor materials, but also produces synergetic benefits such as better visible light harvesting, electron hole separation, and photostability.

3. Proposed study: Genesis and Definition

As stated earlier, semiconductor photoelectrode is the essential component of a conventional PEC system, capturing solar light and promoting redox reactions such as water splitting, CO_2 reduction, and N_2 fixation. A semiconductor photoelectrode can be stimulated by photons with the same or more energy than its band gap energy when exposed to light. The photogenerated holes stay in the valence band, but photogenerated electrons form and split in picoseconds before jumping to the conduction

band. The photo-induced holes and electrons are subsequently steered by the inherent energy band alignment and the applied electric field to the interface between the photoelectrode and the electrolyte. Hydrogen evolution reaction (HER), CO_2 reduction, and N_2 fixation are all triggered by photogenerated electrons. The corresponding holes, in turn, participate in oxidation activities like the oxygen evolution reaction (OER) and the breakdown of organic pollutants. Importantly, a PEC system must have high energy conversion efficiency, high HER and OER reaction rates, long-term stability, operational safety, and low cost for large-scale solar-driven water splitting applications. From the literature survey undertaken (Please see Annexure 1), it is apparent that there exists an important domain of fundamental research, where working with different semiconductor nano-materials, the effects of nanocarbon modifications on PEC performances of the electrodes still need to be investigated in greater detail. Further, in recent years when the thrust is more on combining the advantages of more than one material and to generate a better and more efficient material system for PEC water splitting, the role and significance of nanocarbons has assumed tremendous significance.

Considering all above aspects and promising ideas, proposed study aims to fabricate and evaluate the performance of few bi-layered metal oxide thin film nano-hetero-structures grown onto ITO support. Thin film samples will further be modified by surface incorporation of g-C_3N_4 and/or MWCNT to enhance charge separation and mobility at electrode-electrolyte junction. Promising materials on which the proposed would lay stress for application in PEC water splitting are listed in Table 1.

Table 1: Few promising materials for application as photoelectrode in PEC water splitting.

Materials	**Band gap (eV)**	**CB edge (eV)**	**VB edge (eV)**	**Remarks**
g-C_3N_4	2.7	-1.22	1.5	• 2D-structured metal-free semiconductor • polymeric semiconductor • suitable band edges for water splitting • nontoxic, low cost, simple fabrication, and high physicochemical stability **Limitation** • high recombination rate, poor electronic conductivity, sluggish hole-transfer, limited visible light absorption at long wavelength range of 460 to 760 nm
MWCNT				• Excellent electrical and mechanical properties • large surface area and ability to store electrons and also used as supporter for energy storage and conversion

				• Render the conduction of photogenerated charge carriers and also increases the charge injection and extraction **Limitations** • Expensive • non-uniformity in morphology and structure
$CaFe_2O_4$	1.9	−0.6	1.3	• Inverse spinel • Orthorhombic phase • narrow optical band gap • chemically and thermally stable in neutral or basic solutions • nontoxic, inexpensive and fascinating physicochemical properties **Limitation** • unstable in acidic medium
ZnO	3.2	0.15	3.35	• n-type, Wurtzite phase, direct band gap • High photosensitivity, Photochemical stability, Strong oxidizing power, Non-toxic, low-cost • large exciton binding energy of 60 meV, physical and chemical stable **Limitations** • wide band gap, fast recombination and low quantum efficiency • incomplete visible light harvesting and photocorrosion
$BiVO_4$	2.4	0.46	2.86	• direct band gap • plentiful abundance, low cost, excellent (photo)-electrochemical stability in aqueous solutions and nontoxic **Limitations** • poor electron conductivity and sluggish water oxidation kinetics
TiO_2	3.2	-0.25	2.95	• chemically stable, non-toxic, low cost • suitable band energy levels for the desired water splitting **Limitations** • incomplete visible light harvesting (absorbs only UV light) • wide band gap, fast recombination and low quantum efficiency

The suggested work-plan intends to combine above-mentioned promising materials to produce bi-layered nano-hetero-structured thin films that will be combined with nanocarbon co-catalysts to create efficient photoelectrodes for PEC water splitting. The goal would be to create layered nano-hetero-structured thin films on an ITO glass substrate, with the top layer surface changed either during or after the film is deposited, by nanocarbon incorporation. The resulting films would be thoroughly characterized and investigated for possible use in PEC water splitting.

4. Objectives/stages of the proposed study

The main objectives/stages of the proposed work are listed below:

- Synthesis of layered thin film nano-hetero-structures of chosen semiconductors by wet chemical routes, viz. sol-gel spin coating/spray pyrolysis.
- Surface modifications of the prepared thin film by incorporating nanocarbon co-catalysts.
- Characterization of the prepared film samples by XRD, UV, SEM, EDAX, XPS, TEM and AFM.
- Studies on PEC water splitting using the films prepared and measurement of the performance indicating parameters.

5. Proposed Methodology

For the deposition of thin films onto clean conducting glass substrates (ITO), a wet chemical approach (sol-gel spin coating and spray pyrolysis) would be used. After deposition, films will be sintered at high temperatures to allow the desired crystalline phase to evolve and expand. Surface deposition of nanocarbons co-catalyst onto the produced films will be attempted using various ways. Crystallographic characterization by XRD, optical characterization by UV–Vis spectroscopy, surface morphology by SEM and EDAX analysis, XPS analysis, film thickness by surface profilometer and surface topography by AFM analysis, will be performed on the thus produced surface-modified films. Synthesize samples would be utilized for PEC water splitting by recording the current (I) – voltage (V) plots of the PEC cell under darkness and light, from which photocurrent values would be evaluated.

6. Tentative plan/stages of the proposed work

A tentative plan of the proposed work has been outlined below.

Table 2: Tentative plan of the proposed work

Parameters of the study	**Description**
Preparation of samples Materials of interest	▪ ZnO, TiO_2, $BiVO_4$, $CaFe_2O_4$ ▪ g-C_3N_4, MWCNT
Proposed Avenues for Investigation	▪ Bi-layered nano-hetero-structures grown as ITO supported thin films ▪ Surface modifications induced by incorporating g-C_3N_4, MWCNT
Proposed method for the preparation of samples	Wet chemical process (Sol-gel, spray pyrolysis).

Expected variables in the study	**Preparation of samples:** ▪ Nature of metal oxides and their combinations ▪ Sintering Conditions: Temperature, Environment ▪ g-C_3N_4, MWCNT
Characterization	▪ Phase analysis by XRD ▪ Surface morphology by SEM and EDAX analysis ▪ Surface Topography by AFM ▪ XPS analysis ▪ Band gap energy by UV-Vis spectrophotometer ▪ TEM analysis of selected high-performing samples ▪ Film thickness by surface profilometer ▪ Density ▪ Resistivity ▪ Flatband potential and carrier density
PEC measurement variables	▪ Current-Voltage characteristics of the PEC cell under darkness and illumination. ▪ Photovoltage & Photocurrent ▪ Open circuit potential ▪ Short circuit current ▪ Onset voltage ▪ Applied bias photon to current conversion efficiency (ABPE)

7. Importance of the work and expected outcome

To achieve the ultimate goal of a commercially viable PEC water splitting device for hydrogen generation, research in this critical area should continue in parallel on both aspects, i.e. (i) fundamental research, which explores still unknown and hidden aspects of the phenomenon, and (ii) technology development. The proposed research falls into the first category, as it aims to investigate the promoting effects of inherently conducting carbon-based materials on thin films of metal oxide semiconductors when used as electrodes in PEC water splitting. The work is expected to provide more insight into this hitherto lesser known area of knowledge, and the findings could be used to develop an effective PEC water splitting system for solar-hydrogen generation in the future.

Literature review in the proposed area of work

Baig et al (2020) successfully synthesized visible-light active g- C_3N_4 (CN)-SiC photoanode with distinct SiC concentration by pulsed laser ablation in liquid (PLAL). The as-prepared samples were characterized by different techniques viz. XRD, SEM, TEM, XPS. The photocurrent density of g-CN-SiC photoanode was significantly higher than that of pristine g-CN. The highest photocurrent density

was observed in a sample with a SiC content of 10%, a sevenfold increase was observed compared to pristine graphitic carbon nitride.

Aboubakr et al (2021) successfully prepared P- and S-doped 1D-g-C_3N_4 (CN). A new synthesis method was developed by using supramolecular melamine, ammonium dihydrogen phosphate, and tri-thiocyanuric acid as precursors. XRD and FTIR characterizations showed that the P and S doping of 1D- CN did not affect the skeletal structure of the materials but decreased the crystallinity. The band gap 1D- CN (Eg ≈ 2.4) was decreased after P and S doping. PL spectroscopy revealed that the charge carrier separation was more efficient in 1D-g-C_3N_4 than in bulk 3D-CN, and that the separation was even more effective in 1D-P-CN, and 1D-S-CN. Accordingly, PEC water splitting activity was improved at 1.2 V vs. SCE, the water photo-oxidation current measured at 1D-S- CN was approximately 2.0 and 1.8 times greater, compared to undoped 3D-CN and 1D-CN photoelectrode respectively.

Aboubakr et al (2020) successfully prepared carbonate-intercalated ruptured tubular (RT) structured g-C_3N_4/LDH by co-precipitation of LDH on the surface to escalate the activity of g-C_3N_4 towards PEC oxidation. The specific surface area was increased for photocatalysis of the prepared composites by 13.74 and 9.2-fold compared to RT g-C_3N_4 and LDH, respectively. The PL measurements indicate the capability of the prepared composites to separate electron-hole pairs, which was magnified upto almost 5- & 2-folds with respect to bulk g-C_3N_4 and RT g-C_3N_4. From the PEC water splitting measurements, the generation, separation and transfer of the photo-produced charge carriers were magnified. Moreover, the water oxidation accomplished by g-C_3N_4/LDH composite synthesized was much improved compared to former reported g-C_3N_4/LDH composites.

Babu et al (2020) successfully fabricated Cobalt-doped g-C_3N_4 (Co-g-CN) nanolayer via single-step thermal treatment with urea and cobalt nitrate. Cobalt doping successfully altered the morphological, optical, and band edge potentials of g-CN, resulting in higher PEC performance under visible light. The absorption edge was red shifted by the decrease in the band gap, which improved the light-harvesting properties in the visible region. Co doping also changed the valence and conduction band potentials towards more positive and less negative regions, respectively, and effectively reduced the rate of gathering of e^--h^+ pairs owing to the trapping by Co^{2+} ions, revealed by PL and transient

photocurrent analyses. Optimized Co doped samples showed photocurrents approximately 1.8 times larger than g-CN as well as higher high electrical conductivity. The PEC performance of g-CN was significantly improved by cobalt doping due to the formation of a layered structure and the presence of Co^{2+} ions in the 2-D matrix.

Babu et al (2020) successfully synthesized a novel g-C_3N_4/Au-SnO_2 quantum dot (g-CN/Au-SQD) ternary nanocomposite in a three-step process for the degradation of the organic pollutant rhodamine B (RhB), and photoelectrochemical (PEC) water splitting under visible light illumination. Au-SQDs were prepared via a one-pot chemical reduction method, and g-CN was synthesized via the thermal polymerization of urea at 550 °C. The g-CN/Au-SQD ternary nanocomposite was prepared via sonication, stirring, and finally annealing. This method was effective in the mixing and dispersing of Au-SQDs over the whole surface of the two-dimensional (2D) g-CN nanosheets. The light-capturing capability was enhanced and optimized with the loading of distinct amounts of Au-SQDs. The bandgap was reduced from 2.85 eV (g-CN) to 2.58 eV (g-CN/Au-SQD). Photoluminescence analysis revealed the inhibited nature of recombination of e^--h^+ in the ternary nanocomposites. The CNAS-20 photoelectrode showed lower charge-transfer resistance than other prepared samples, suitable for PEC water splitting. The CNAS-20 photoelectrode showed a significant photocurrent, which was a ~3.83 time larger than that of pure g-CN.

Chaudhary et al (2020) synthesized organic/inorganic TiO_2/C_3N_4/CNT photoanode by hydrothermal method. The TiO_2/C_3N_4/CNT photoanode showed a photocurrent density of 2.94 mA/cm^2, which was ~6.4 time better than pristine C_3N_4 at an applied bias potential of 0.6 V vs. Ag/AgCl. The highest photocurrent density of ternary photoanode was creditable to the heterojunction formation at TiO_2/ C_3N_4 interfaces and the presence of CNT advanced the rapid transfer of charge carriers. The TiO_2/C_3N_4/CNT photoanode showed an onset potential of 0.25 V vs. Ag/AgCl which was significantly lower compared to pristine C_3N_4 and TiO_2/C_3N_4 nanocomposite. The interface barrier height (~10 meV) between TiO_2 and C_3N_4, attained from Kelvin probe force microscopy results, implied that the migration of electrons was favoured through TiO_2/C_3N_4 interfaces in a ternary photoanode. The smaller amount of charge transfer resistance (R_{ct} = 9.4 kΩ) for TiO_2/C_3N_4/CNT photoanode indicates a fast charge transfer rate, which enhances it to achieve maximum photocurrent density.

Fang et al (2019) developed a polymeric carbon nitride (PCN) based visible-light sensitive photoanodes with gradient sulphur doping along the films by conventional molten mediate polymerization. The formed band structure of PCN films was extensively investigated, and it was found that sufficient charge separation and transfer took place and visible light absorption of the films was elevated up to 2.55 eV. The optimal photoanode accquired the photocurrent density of 110 $\mu A/cm^2$ at 1.23 VRHE under AM 1.5 illumination in 1.0 M NaOH solution.

Ghane et al (2020) prepared a g-C_3N_4/Fe_2O_3 nanocomposite by the solution combustion synthesis (SCS) of iron-nitrate/g-C_3N_4 mixtures of different concentration ratios and using urea as a fuel. The attachment of Fe_2O_3 nanoparticles to the g-C_3N_4 by chemical and hydrogen bonds resulted in visible light-harvesting, electron-hole recombination reduction, and bandgap compression. Under visible-light, the CNFe-1.21 showed twelve times greater photocurrent density than pure g-C_3N_4. The noticeable photo response and catalytic effects of the prepared nanocomposites were attributed to the amplification of the specific surface area and the enhanced light absorption and the diminished electron-hole recombination all because of the solution combustion reactions. Increasing the Fe_2O_3 content of the nanocomposite enriched its photo response, but excessive Fe_2O_3 content detracted the achieved gain due to nanoparticle agglomeration and the achieved electron mobility attenuation.

Guigoz et al (2020) constructed a $LaFeO_3$/g-C_3N_4 film via magnetron sputtering and g-C3N4 was deposited directly on the substrate, prior to $LaFeO_3$, using a simple spin-coating method. Deposition of a sublayer of g-C_3N_4 enhances the separation of charge carriers at the $LaFeO_3$/g-C_3N_4 interface. The $LaFeO_3$/g-C_3N_4 film was characterized by various techniques including SEM, XRD, Raman spectroscopy, XPS and photo-electrochemical measurements. The hydrogen production rate of a g-C_3N_4 film coated with $LaFeO_3$ film, showing both 50 nm thickness, was 10.8 mmol h^{-1} cm^{-2} under visible light irradiation, 70% higher than measured for pure $LaFeO_3$ and g-C_3N_4 films and confirms the effective separation of electron-hole pairs at the interface of $LaFeO_3$/g-C_3N_4 films. Furthermore, the $LaFeO_3$/g-C_3N_4 films were stable and retained a high activity (70%) after a third reuse.

Guru et al (2020) fabricated a nanocomposite BOC/NiFe-LDH@g-C_3N_4 (15 wt% of g-C_3N_4) by co-precipitation method. The XPS and powder XRD studies revealed that Bi was anchored on NiFe-LDH plates in $Bi_2O_2CO_3$ form. NiFe-LDH photoanode acquires bifunctional character due to $Bi_2O_2CO_3$

agglomerates and g-C_3N_4 embedded in the BOC/NiFe-LDH@g-C_3N_4. The onset potential of BOC/NiFe-LDH@g-C_3N_4 for HER appears at η = 0.245 V in dark and η = 0.217 V in light; and for OER, it appears at η = 0.340 V in dark and η = 0.234 V in light after 30 min exposure. The IPCE at 525 nm, TOF and theoretical yield are estimated considering 100% faradaic efficiency and assuming all the active sites participate in both HER and OER. For HER η = 0.27 V, the nanocomposite BOC/NiFe-LDH@g-C_3N_4 shows 3% IPCE, 0.08 s^{-1} TOF and 9.89 mmol theoretical yield after 30 min exposure to light. For OER η = 0.39 V, it shows 12% IPCE, 0.19 s^{-1} TOF and theoretical yield of 23.7 mmol after exposure to 30 min light.

Hosseini H. et al (2020) successfully developed CuO/graphitic carbon nitride (g-C_3N_4) nanocomposite under microwave irradiation. A simple, one-pot method was used to directly deposit the nanocomposite onto FTO from a solution containing copper precursor and urea. The bandgap engineering due to C-doping and creation of defect sites by the introduction of Cu–C or Cu–O–C chemical bonds, reduced Eg and led to improved light absorption, decreased recombination rate, and ultimately increased rate of electron-hole photo-generation. The results of PEC studies demonstrated C-doped CuO/g-C_3N_4 heterojunction not only showed a significantly improved water splitting performance of almost 3.3 times higher than CuO but also signifiantly improved the photocorrosion stability over a long period. Also, the hydrogen evolution rate was significantly enhanced from 2.352 µmol $h^{-1}cm^{-2}$ for CuO to 3.13 µmol $h^{-1}cm^{-2}$ for C-doped CuO/g-C_3N_4.

Li et al (2020) successfully fabricated C_3N_4/$BiVO_4$ hybrid electrodes by incorporating g-C_3N_4 into the nanoporous $BiVO_4$ using a simple in-situ synthesis method. With an optimal loading of g-C_3N_4, the 2-C_3N_4/$BiVO_4$ electrode showed a high photocurrent density of 4.06 mA/cm^2 at 1.23 V (vs. RHE) for water oxidation, an improvement of 2.8 times higher than that of the $BiVO_4$. The improved PEC performance of the g-C_3N_4 photoanodes by simultaneously promoting the charge separation and surface reaction kinetics. When a NiOOH co-catalyst was immobilized onto the 2-C_3N_4/$BiVO_4$ electrode, both the PEC property and photoanode stability were improved. The remarkably high photocurrent density of 5.44 mA/cm^2 at 1.23 V was obtained. The largest half-cell solar energy conversion efficiency for NiOOH/2-C_3N_4/$BiVO_4$ was 1.43% at 0.78 V, corresponding to 8.4 times the unmodified $BiVO_4$ (0.17% at 0.97 V).

Mohamed et al (2021) synthesized g-C_3N_4/ThO_2 (~5.8%) via thermal treatment and g-C_3N_4 polymerization (precursor: Urea, 30 min; 520 ˚C showed remarkable and high photocatalytic activity. The photocurrent density reached for g-C_3N_4/ThO_2 was 9.71 μcm^{-2} at 1.23 V vs. Ag/ AgCl under simulated light (100 mW/cm^2) that was more than twice compared with the undoped g-C_3N_4 (~4.23 μA cm^{-2}). The doping with ThO_2 (~5.8%) indicated an improvement in photo-generated charge transfer and in separation. The contribution of Th^{4+} and O^{2-} doping on the g-C_3N_4 was also confirmed by the result of XPS, PL spectra, FESEM image, XRD, FTIR, UV–Vis, and TGA. The recombination inhibition of the photogenerated carriers in the polymer itself (g-C_3N_4) via Th^{4+} and O^{2-} doping accelerated the charge transportation.

Reddy et al (2021) synthesized g-C_3N_4 nanostructures and Sr-doped g-C_3N_4 to check the PEC water splitting performance in visible light. Spectroscopy analysis examination revealed the inclusion of Sr^{2+} into the g-C_3N_4 host lattice. Under selective Sn doping, the impedance study revealed promising charge carrier kinetics. Gentle doping of Sr (0.4 mol %) into g-C_3N_4 resulted in a significant increase in photocurrent production, which was 82 times higher than bare g-C_3N_4.

Reddy et al. (2020) used a two-step solvo-thermal procedure in an aqueous phase to produce a highly efficient and stable g-C_3N_4-decorated CdS-nanoparticle-doped Fe_3O_4 nanocube catalyst, g-C_3N_4@CdS–Fe_3O_4 (gCNCSF). By calcining melamine and isolated onion leaf extract at 450°C in a N_2 environment, g-C_3N_4 was produced. Following that, a CdS@Fe_3O_4 catalyst was created by hydrothermally doping of CdS nanoparticles into the Fe_3O_4 interfacial layers and calcining at 450 °C under N_2. The photocurrent density of the gCNCSF catalyst was 0.023 mA/cm^2 at 0.2 V vs. Ag/AgCl, which was 2.5 and 6.25 times greater than that of the binary hybrids g-C_3N_4@CdS and CdS@Fe_3O_4, respectively. Furthermore, the performance of neat CdS and g-C_3N_4 was approximately 4.1 and 27.7 times greater, respectively, than that of neat CdS and g-C_3N_4.

Reddy et al. (2021) used thermal treatment of urea and ammonium metavanadate to successfully produce undoped and V-doped g-C_3N_4 nanosheets. The efficient incorporation of the V dopant into the host g-C_3N_4 lattice was validated by the structure, morphology, and optical characteristics. The morphological and optical features of g-C_3N_4 were strongly impacted by the dopant substance. With increasing dopant concentration, the optical band-gap dropped from 1.81 to 1.67 eV. Furthermore, the

doped g-C_3N_4 samples had higher photocatalytic activity than the undoped samples. The maximum photocurrent density of the 0.3 mol % V doped g-C_3N_4 (0.3 V) photoelectrode was 0.80 mA cm^{-2}, which was 40 times greater than that of the pure g-C_3N_4 sample, and it had improved stability for 310 seconds.

Rouby et al. (2020) used direct pyrolysis of supramolecular melamine to make a Bi-doped g-C_3N_4 elongated nano-structure sample. P-XRD, FTIR, SEM, TEM, EDX, DRS, and PL methods were used to describe the samples. The 2.5 % Bi-g-C_3N_4 photoanode's high photoelectrocatalytic activity was attributed to its improved crystallinity, adequate band gap energy (2.24 eV) and band locations, and high capacity to inhibit electron-hole recombination (the PL peak intensity was quenched 6-times compared to the reference material, pristine g-C_3N_4). LSV and PEIS measurements were used to assess the performance of pure and Bi-doped g-C_3N_4 samples. The photocurrent measured on the 2.5 % Bi-doped sample was two times more than the un-doped sample.

Seo et al (2020) used a simple hydrothermal synthesis to create a Tin dioxide (SnO_2) nanoflakes electrode, which was then coated with a g-C_3N_4 layer by electrophoretic deposition, which was varied by altering the deposited time from 3 to 10 minutes to change the PEC performance. In the g-C_3N_4 (5min)/SnO_2 nanoflakes electrode, the greatest JSC of 0.15 mA/cm^2 at 1.23 VRHE was reached under full sun and a modest photoresponse in visible light of 400-450 nm adds to the augmentation of JSC when compared to that of SnO_2 nanoflakes film.

Ahmed et al. (2019) used hydrothermal and chemical vapour deposition to synthesize a nanohybrid carbon nanotubes@TiO_2 nanoribbons (CNTs@TNRs) photoelectrode that was tested in different electrolytes for PEC water splitting. Different techniques were used to characterise the prepared samples. The crystallite size of the CNTs@TNRs nanohybrid has been raised from 14.86 nm for TNRs to 21.61 nm for CNTs. In comparison to TNRs, the absorption area of CNTs@TNRs was pushed to visible light, with band gaps of 3.78 eV and 2.07 eV for TNRs and CNTs@TNRs, respectively. The prepared samples were evaluated in varied amounts of $Na_2S_2O_3$, HCl, and KOH electrolytes. The photocurrent density density in different electroltes can be sorted in the following order: JKOH > J$Na_2S_2O_3$ > JHCl. At 510 nm, the 97 % IPCE was computed, which was higher than previously

reported photoelectrodes. CNTs@TNRs photoelectrode had the highest photocurrent density of 102 $mAcm^{-2}$ and 300 mmol h-1 cm^{-2} hydrogen evolution rates.

Anson-Casaos et al. (2020) deposited carbon dots (CDs) on TiO_2 using a variety of approaches, including microwave irradiation, hydrothermal conditions, and solution chemistry at room temperature followed by chemical functionalization. When CDs were functionalized with thiol groups and butyl chains, the photocurrent density increased. The IPCE value improved, and absorption expanded by 20 nm toward longer wavelengths. For c-TiO_2/m-TiO_2 + But-CD electrodes, the greatest photocurrent was observed and was steady for continuous operation.

Bae et al. (2020) used a simple, affordable, and scalable electroless technique to make a CNT;Pd-Ni based Si photocathode for acidic water splitting. Si photocathode based on CNT;Pd-Ni could be a viable replacement for platinum photocathode in hydrogen evolution reactions. At a photocurrent density of 10 mA/cm^2, the greatest photocurrent density was found at 35 mA/cm^2 with overpotential of – 0.04 V (vs. RHE). Due to the formation of Pd-Ni alloy on the surface of carbon nanotubes, the total charge transfer resistance decreases, resulting in greater band bending and, ultimately, improved Si photocathode PEC performance.

Fan et al. (2019) used an electrodeposition approach to create a $BiVO_4$-N/C-CoPOM photoanode. Due to modification by N-doped carbon and cocatalyst CoPOM loading, the photocurrent density was raised by 5.4-fold (3.30 mA cm^{-2} at 1.23 V vs. RHE) as compared to pure $BiVO_4$. The $BiVO_4$-N/C-CoPOM photoanode had the greatest ABPE value of 1.22 % at a low voltage of 0.63 V vs. RHE. The high charge injection efficiency of 90.26 % at 1.23 V vs. RHE and the low onset potential of the photocurrent show that loading of CoPOM cocatalyst alleviated the problem of sluggish hole transfer kinetics of BiVO4, as evidenced by the high charge injection efficiency of 90.26 % at 1.23 V vs. RHE and the low onset potential of the photocurrent. As a result, it's thought that a new POM cocatalyst might be utilized to improve PEC water oxidation, perhaps opening up a new path for solar energy.

Gadisa et al. (2020) used a hydrothermal technique to create a modified ZnO@Ni foam (NF) photoelectrode by heteroatom (O, S, and N) doping in graphitic carbon, which provided extractive sites for the OER process. The diffusion of ions and the kinetics of surface reactions were aided by the growth of a flower-like carbon structure on ZnO nanorods, which enhanced the active surface area.

Because of its greater photocurrent response and lower overpotential, ZnO-C@NF may be a better alternative than clean ZnO@NF.

Kim et al. (2020) used a supersonic cold-spray deposition approach to make a Zn_2SnO_4/SnO_2/carbon nanotube (CNT) for PEC water splitting. In comparison to lower, greater, or no CNT content, PEC performance was better in the 1:3 CNT to Zn_2SnO_4 ratio. A rather high photocurrent density of 17.2 mA cm-2 was observed at a modest applied potential of 0.76 V vs. Ag/AgCl. It is possible to improve photoanode PEC performance simply by adjusting and optimising carbon nanotube concentration.

Liao et al (2021) developed a TiO_2/NCD/Au (ternary titanium dioxide/ nitrogen-doped carbon dot/gold) photoanode. TiO_2/NCD/Au, TiO_2/NCD, and TiO_2/ Au photoelectrodes had photocurrent densities of 10.26 mA/cm^2, 7.55 mA/cm^2, and 4.34 mA/cm^2 correspondingly. Transient photovoltage (TPV) testing revealed that NCDs and Au had a synergistic impact in improving TiO_2 charge carrier separation efficiency. As a result, the TPV approach can be used to quickly and efficiently analyse electron generation and transit in a light response system.

Sial et al. (2021) used a hydrothermal approach followed by a drop-casting method to synthesize a nitrogen-doped carbon dots (NCDs)/WO_3 photoelectrode. The synthesised NCDs appear to be 3 nm in size with a homogeneous distribution over WO_3 NRs, according to the results of the characterization. When compared to bare WO_3, optical experiments revealed that WO_3 NRs/NCDs have a higher light absorption potential. At 1.23 V vs. RHE, the optimal amount of NCDs loading on WO_3 NRs produced the maximum photocurrent density of 1.54 mA cm^{-2}. IPCE measurements for the WO_3 NRs/NCDs heterojunction revealed higher light absorption in the UV area (300-400 nm) as well as extended absorbance in the visible light range (500 nm-600 nm), both of which contributed to increased PEC activity. Furthermore, the phase mode technique of Kelvin probe force microscopy and electrostatic force microscopy (KPFM and EFM) was used to image the change in charge concentration at the WO_3 surface before and after the NCDs deposition, which supports the device's improved PEC activity.

Wang et al. (2021) created a photoelectrode with carbon quantum dots (CQDs) loaded on $NiTiO_3$ (NTO) for water oxidation (WOR). In a power-based photocatalytic system, performance was boosted 7-fold over pure NTO, and significant stability was achieved by preserving the output for at least 10 hours. The CQDs were shown to load on an NTO-based photoanode for WOR, resulting in a 6-fold

increase. In-situ characterizations were performed to investigate the roles of CQDs in WOR, and it was discovered that CQDs can aid in the chemical adsorption of water molecules while also promoting the generation of hydroxyl radicals as WOR transition states. This demonstration provides a hint to understanding the role of carbon in photocatalytic systems, which will help to promote WOR and its usage in advanced photoredox catalytic reactions.

Zhao et al. (2018) developed a UV-Vis-NIR broad spectrum carbon dots modified WO_2-Na_xWO_3 (WO_2-Na_xWO_3-CDs) photocatalyst for water splitting. When 0.008 g-CDs/g-catalyst conc. was used, the maximum photocatalytic activity was observed. Under UV (420 nm), Vis (420 nm760 nm), and NIR (>760 nm) light irradiation, the stoichiometric ratio of H_2 evolution and O_2 evolution, as well as the H_2/O_2 evolution rates, are 0.05/0.02, 2.58/1.24, and 4.74/2.28 mol/h, respectively. For at least 6 rounds of repeating testing, WO_2-Na_xWO_3-CDs demonstrated outstanding stability. The excellent photocatalytic activity of the as-prepared WO_2-Na_xWO_3-CDs can be attributed to the synergistic effect of WO_2-Na_xWO_3 and CDs, in which WO_2-Na_xWO_3 provides the appropriate band-gap while CDs extend the photo-responding range, speed up electron transfer, and improve photo-induced charge carrier separation efficiency. The established hybrid photocatalytic system provides a new technique for designing broad spectrum absorption photo catalysis systems to increase solar light usage.

Xiao et al (2021) used candle flame treatment to create carbon coated-CuO-Cu_2O photocathode conductive copper foam (C-CuO-Cu_2O/CF) for PEC water splitting. With a photocurrent density of 1.2 mA cm^{-2} at 0V RHE, the C-CuO-Cu_2O/CF photocathode displayed increased photoelectrochemical activity. As demonstrated by M-S, IPCE, and EIS results, the high performance of the prepared photocathode is due to the unique surface carbon coating and CuO-Cu_2O interface, which can increase carrier concentration, reduce carrier recombination rate, and enhance charge transfer at the photocathode/electrolyte interface. C-CuO-Cu_2O/CF is an appealing photocathode for PEC applications because of its greatly increased activity.

Zhou et al. (2020) used a hydrothermal approach to create a carbon quantum dots (CQDs) modified anatase/rutile TiO_2 photoanode (CQDs/A/R-TiO_2). The A/R-TiO_2 heterojunction considerably reduced bulk recombination of photogenerated carriers, according to the findings. With the addition of CQDs to A/RTiO_2, OER kinetics and ultraviolet–visible (UV–Vis) light harvesting were greatly improved.

At 0.6 V vs. RHE, the bulk charge separation efficiency (η_{bulk}) and surface charge injection efficiency ($\eta_{surface}$) of CQDs/A/R-TiO_2 are 1.69 and 5.74 times greater, respectively, than that of pristine TiO_2. Meanwhile, for CQDs/A/RTiO_2, the photocurrent was boosted by 11.72 times and the onset potential was moved by 240 mV.

Abd-Elrahim et al (2021) et al created ZnO-graphene nanosheets coated on titanium sheets from micro-sized ZnO and graphite powder by using a spray pyrolysis process. The photo-response current @1.23 V vs. RHE of the ZnO-graphene NCs/Ti-sheet hybrid photoanodes with 25, 50, and 75 wt % graphite content, respectively, was 1.69, 4.82, and 2.6 mA/cm^2, compared to 0.47 mA/cm^2 for the nanosized ZnO/Ti-sheet photoanode. In comparison to ZnO/Ti-sheet photoanodes, the maximum IPCE for ZnO-graphene NCs/Tisheet hybrid photoanodes has been adjusted to a lower potential. At the smallest bias potential of 1.4 V vs. RHE, the NCs hybrid photoanode with 50% graphite component had the maximum efficiency of 4.23 %. For all constructed photoanodes, the photocurrent stability was tested for ten cycles.

Atacan et al. (2020) used a precipitation approach to make unique Ag_2CrO_4/GO/$MnFe_2O_4$ photocatalysts, which were then electrophoretically deposited on ITO. Microscopic examination, chemical, and structural investigations were used to verify the Ag_2CrO_4/GO/$MnFe_2O_4$ composite. Compared to $MnFe_2O_4$, GO, Ag_2CrO_4, and GO/$MnFe_2O_4$, ternary composite had a greater photocurrent response and a poorer photoluminescence spectrum. Under visible light illumination, the best photoelectrochemical hydrogen generation result in the presence of Ag_2CrO_4/GO/$MnFe_2O_4$ composite was determined to be 446.93 $mmol.cm^{-2}$ in 90 min. Because of its high photoactivity, low cost, and environmental friendliness, Ag_2CrO_4/GO/ $MnFe_2O_4$ was used to boost photoelectrochemical hydrogen evolution.

Kawrani et al (2020) created a $CaCu_3Ti_4O_{12}$ (CCTO) visible light active electrode (CuO) due to its exceptional structure in which CCTO encloses a visible light absorbance component. The trapping of electrons was mostly due to the presence of CuO on the material surface. As a result, varying quantities of graphene oxide (GO) were used to make CCTO photoelectrocatalysts in this study. XRD, SEM, XPS, and Raman characterizations demonstrated that the oxidation of GO at high temperatures resulted in the reduction of Ti^{4+} to Ti^{3+} and Cu^{2+} to Cu^{+}, resulting in a segregation of copper on grain

boundaries regions. In the dark and under visible light irradiation, electrochemical performance and material resistance were measured. The photocurrent generation and hydrogen generation rate of CCTO produced with 3% GO were 50 % higher than the pure phase of CCTO. The hydrogen generation yield was evaluated, and the findings showed that for the sample prepared with 3wt. % of GO, the rate of hydrogen generation increased to 2.9 mol/h, which was 50% greater than the rate of hydrogen generation using pure CCTO.

Sajjadizadeh et al. (2019) developed a photoanode (Ni (OH) $_2$ photoanode) with a cascade structure of FTO|c-TiO_2|few graphene layers|TiO_2/GQDs|$Ni(OH)_2$ assembly. In the photo-electrocatalytic oxygen evolution process, this photoanode had substantially lower electron-hole recombination, quick charge transport, better visible light harvesting, and good performance compared to FTO|c-TiO_2|TiO_2 construction (TiO_2 photoanode). The photocurrent density of the Ni (OH) $_2$ photoanode was 7 times that of the TiO_2 photoanode (0.35 mA cm^{-2} at 1.23 V vs. RHE) (0.045 mA cm^{-2} at 1.23 V vs. RHE). In the Ni (OH) $_2$ photoanode, the compact TiO_2 (c-TiO_2) layer acts as an effective hole-blocking layer. The transit of photogenerated electrons from the TiO_2/GQDs conduction band to FTO could be speed up by a few-layer graphene layer. The Ni (OH) $_2$ layer was capable of rapidly transferring holes into the electrolyte solution.

Zargazi et al (2021) created a new morphology of 3D inverse opallike UiO-66 films by infiltrating UiO-66 sol into a colloidal PS template. As a new design of photoelectrode for PEC water splitting, the resultant 3D inverse opal-like UiO-66 films were systematically decorated with Pd nanoparticles and S, N graphene quantum dots (GQDs). The photoanode made of UiO-66/Pd/S, N GQDs, showed a photocurrent density of 300 A /cm^2 at 1.23 V vs RHE under AM 1.5G. Under visible light at 500 nm, the applied bias photon-to-current efficiency (ABPE) is 0.66 % at 0.65 V vs RHE, and the absorbed photon-to-electron conversion efficiency (APCE) is 19.7%. The engineering of the band gap and effective decrease of charge transfer resistance of MOF with the addition of Pd nanoparticles resulted in this high efficiency.

Bai et al. (2020) used ordinary chemical vapour deposition (CVD) and metal-organic decomposition, followed by spin-coated rGO on the SnO_2/$BiVO_4$ junction, to create a ternary photoanode of SnO_2/$BiVO_4$/rGO. At 1.23 V vs. RHE, the ternary photoanode produces the maximum photocurrent

density of 2.05 mA cm^{-2}, which is 3.73 times that of the $BiVO_4$ photoanode (0.55 mA cm^{-2}). At 400 nm, the ternary photoanode's incident photon-to-electron conversion efficiency (IPCE) is 2.47 times that of the $BiVO_4$ photoanode, and the onset potential has a cathodic shift of 300 mV.

Elbakkay et al (2021) used a hydrothermal technique to manufacture TiO_2 nanoparticles sensitised with rod-like Sb_2S_3 (stibnite) on the surface of a reduced graphene oxide (TiO_2/Sb_2S_3/RGO) photoanode. The TiO_2/Sb_2S_3, TiO_2/Sb_2S_3/5 % RGO, and TiO_2/Sb_2S_3/10 % RGO hybrid electrodes absorbed light with a broad absorption band edge extending to 750 nm. The TiO_2/Sb_2S_3/10% RGO photoanode produced the highest photocurrent density, which were 400 % higher than that of a pure TiO_2 photoanode and 200 % higher than that of the TiO_2/Sb_2S_3 photoanode.

Ghasemi et al (2021) developed a photoanode made of reduced graphene oxide, molybdenum disulfide, and gold nanoparticles (rGO/MoS_2/Au NPs). Modified Hummers' and solvent-based sonication procedures were used to make the GO and MoS_2 dispersions, respectively. rGO/ MoS_2 heterostructures were fabricated on FTO substrates using the casting procedure. After that, 5 nm of Au was deposited on the electrode, and a thermal-assisted treatment was used to create the final photoanode (rGO/ MoS_2/Au NPs). SEM, TEM, Raman, UV–Visible, and AFM techniques were used to investigate the inserted heterostructure. The photocurrent density of the rGO/MoS_2/Au NPs heterostructure is around 240 % higher than that of the GO/MoS_2 hybrid, owing to the effective transfer of electrons to Au NPs and a significant reduction in the recombination rate of photogenerated carriers.

Sharma et al. (2021) used a thermal evaporation method to create a SnS thin film on an ITO glass substrate, followed by a drop cast process to install a reduced graphene oxide (rGO) layer. The photoelectrochemical activity of the samples was examined using XRD, Raman, SEM, and UV-Visible absorption spectroscopy. The results revealed the development of pure phase SnS with an orthorhombic crystal structure and an optical band gap of 2.0 eV, with the absorption in the visible range being enhanced by the rGO layer. At 0.95V Ag/AgCl, SnS/0.1 wt % rGO displayed a maximum photocurrent density of 1.1 mA/cm^2 compared to pristine SnS (0.3 mA/cm^2) with improved photostability up to 1 h.

Tang et al (2020) developed a novel Cu_2O nanoparticles / Bi_2WO_6 / reduced graphene oxide (Cu_2O NPs / BWO / rGO) hybrid by a facile solvothermal synthesis followed by chemical reduction. Cu_2O NPs and rGO distributed evenly over hydrangea-like BWO. This novel hybrid shows 14 times the improved PEC performance of the current image density higher than that of pure BWO under solar radiation. This improvement in PEC performance is due to significant improvements in the integration of Cu_2O NPs with rGO, which proves the Z-scheme as a key driver in Cu_2O NPs / BWO, and rGO as an important charger bridge for effective cost-effectiveness, as well as increased visual absorption of light.

Yaw et al (2019) designed and validated a novel V_2O_5/rGO/ $BiVO_4$ heterojunction photoanode. The use of an efficient charge transport medium-rGO interlayer between a proven V_2O_5/$BiVO_4$ heterojunction photoanode enhanced light harvesting efficiency and electronic transmission performance across the V_2O_5/$BiVO_4$ heterojunction photoanode, which can suppress electron-hole pair recombination. As a result, the photocurrent density generation potential was altered by the adjustable amount of drop-casted rGO interlayer. The ternary V_2O_5/i-rGO/$BiVO_4$ i= 4) heterojunction photoanode had the maximum photocurrent density of 2.1 mA/cm^2 at 1.5 V vs. Ag/AgCl, which was roughly 9.7 times more photoactive than pristine $BiVO^4$ among the as-prepared samples. The increased efficiency of the ternary nanostructured V_2O_5/rGO/$BiVO_4$ heterojunction photoanode was further confirmed by the H_2 evolution rate.

Zhang et al (2021) constructed a ternary WO_3/RGO/Ni:FeOOH photoanode, with Ni:FeOOH acting as a bi-functional modifier and RGO acting as a conductive bridge-linker. When compared to the WO_3 NFs at 1.23 V vs. RHE, the photocurrent density of the WO_3/RGO/Ni:FeOOH was 1.32 mA /cm^2 aggrandized by 2.05-fold, with an 83 mV cathodic shift of onset potential. These findings showed that PEC response occurs only in Ni:FeOOH and not in FeOOH. As a result, by creating a p-n heterojunction with the WO_3 NFs, Ni:FeOOH, serving as a bi-functional modifier, can not only boost light absorption but also promote charge transfer. Furthermore, by establishing a continually conducting network, RGO can optimise the charge separation process even more. Faradaic efficiency and stability are both enhanced by their synergistic effects.

References

- Abd-Elrahim, A.G. and Chun, D.M. (2021) Facile one-step deposition of ZnO-graphene nanosheets hybrid photoanodes for enhanced photoelectrochemical water splitting. *J Alloys Compd.*, *870*, 159430.
- Aboubakr, A.E.A., El Rouby, W.M., Khan, M.D., Farghali, A.A. and Revaprasadu, N., (2020) ZnCr-CO_3 LDH/ruptured tubular g-C_3N_4 composite with increased specific surface area for enhanced photoelectrochemical water splitting. *Appl. Surf. Sci.*, 508, 145100.
- Aboubakr, A.E.A., El Rouby, W.M., Khan, M.D., Revaprasadu, N. and Millet, P. (2021) Effect of morphology and non-metal doping (P and S) on the activity of graphitic carbon nitride toward photoelectrochemical water oxidation. *Sol. Energy Mater Sol. Cells*, *232*, 111326.
- Ahmed, A.M., Mohamed, F., Ashraf, A.M., Shaban, M., Khan, A.A.P. and Asiri, A.M. (2020) Enhanced photoelectrochemical water splitting activity of carbon nanotubes@ TiO_2 nanoribbons in different electrolytes. *Chemosphere*, *238*, 124554.
- Ansón-Casaos, A., Hernández-Ferrer, J., Vallan, L., Xie, H., Lira-Cantú, M., Benito, A.M. and Maser, W.K. (2021) Functionalized carbon dots on TiO_2 for perovskite photovoltaics and stable photoanodes for water splitting. *Int. J. Hydrog. Energy*, *46*(22), 12180-12191.
- Atacan, K., Güy, N., Boutra, B. and Özacar, M. (2020) Enhancement of photoelectrochemical hydrogen production by using a novel ternary Ag_2CrO_4/GO/$MnFe_2O_4$ photocatalyst. *Int. J. Hydrog. Energy*, *45*(35), 17453-17467.
- Babu, B., Koutavarapu, R., Shim, J. and Yoo, K. (2020) Enhanced visible-light-driven photoelectrochemical and photocatalytic performance of Au-SnO_2 quantum dot-anchored g-C_3N_4 nanosheets. , *Sep. Purif. Technol. 240*, 116652.
- Babu, B., Shim, J. and Yoo, K. (2020) Efficient solar-light-driven photoelectrochemical water oxidation of one-step in-situ synthesized Co-doped g-C_3N_4 nanolayers. *Ceram. Int.*, 46(10), 16422-16430.
- Bae, H., Burungale, V., Park, J.B., Bang, S.W., Rho, H., Kang, S.H., Ryu, S.W. and Ha, J.S. (2020) Pd-Ni nanoalloy decorated carbon nanotubes based efficient and stable silicon

photocathode for acidic water splitting. *Appl. Surf. Sci.*, *510*, 145389.

- Bai, S., Tian, K., Meng, J.C., Zhao, Y., Sun, J., Zhang, K., Feng, Y., Luo, R., Li, D. and Chen, A. (2021) Reduced graphene oxide decorated $SnO_2/BiVO_4$ photoanode for photoelectrochemical water splitting. *J. Alloys Compd.*, *855*, 156780.
- Baig U., Khan A., Gondal M.A., Dastageer M.A., Akhtar S. (2021) Single-step synthesis of silicon carbide anchored graphitic carbon nitride nanocomposite photo-catalyst for efficient photoelectrochemical water splitting under visible-light irradiation, *Colloids Surf. A Physicochem. Eng.*, 20; 611:125886.
- Bak T., Nowotny J., Rekas M., Sorrell C. (2002) Photo-electrochemical hydrogen generation from water using solar energy, *Int. J. Hydrog. Energy*, 27, 991–1002.
- Chaudhary, D., Kumar, S. and Khare, N. (2020) Boosting the visible-light photoelectrochemical performance of C_3N_4 by coupling with TiO_2 and carbon nanotubes: An organic/inorganic hybrid photocatalyst nanocomposite for photoelectrochemical water spitting. *Int. J. Hydrog. Energy*, *45*(55), 30091-30100.
- Chiam, S.Y., Kumar, M.H., Bassi, P.S., Seng, H.L., Barber, J. and Wong, L.H., (2014) Improving the efficiency of hematite nanorods for photoelectrochemical water splitting by doping with manganese. *ACS appl. Mater. Interfaces*, *6*(8), 5852-5859.
- Dass S., Satsangi V.R., and Shrivastav R. (2000). Solar Energy Induced Hydrogen: Photochemical Way. Chemistry Education Rev., 15(3), 5-12
- El Rouby, W.M., Aboubakr, A.E.A., Khan, M.D., Farghali, A.A., Millet, P. and Revaprasadu, N. (2020) Synthesis and characterization of Bi-doped g-C_3N_4 for photoelectrochemical water oxidation. *Sol Energy*, *211*, 478-487.
- Elbakkay, M.H., El Rouby, W.M., Mariño-López, A., Sousa-Castillo, A., Salgueirino, V., El-Dek, S.I., Farghali, A.A., Correa-Duarte, M.A. and Millet, P. (2021). One-pot synthesis of TiO_2/Sb_2S_3/RGO complex multicomponent heterostructures for highly enhanced photoelectrochemical water splitting. *Int. J. Hydrog. Energy*, *46*(61), 31216-31227.
- Fan, K., Chen, H., He, B. and Yu, J., 2020. Cobalt polyoxometalate on N-doped carbon layer to

boost photoelectrochemical water oxidation of $BiVO_4$. *Chem. Eng. J.*, *392*, 123744.

- Fang, Y., Li, X., Wang, Y., Giordano, C. and Wang, X. (2020) Gradient sulfur doping along polymeric carbon nitride films as visible light photoanodes for the enhanced water oxidation. *Appl. Catal. B.*, *268*, 118398.
- Fujishima, K. J.A, and Honda, K. (1972) Electrochemical photolysis of water at semiconductor electrode, *Nature*, 238, 37-38.
- Gadisa, B.T., Baye, A.F., Appiah-Ntiamoah, R. and Kim, H. (2021) ZnO@ Ni foam photoelectrode modified with heteroatom doped graphitic carbon for enhanced photoelectrochemical water splitting under solar light. *Int. J. Hydrog. Energy*, *46*(2), 2075-2085.
- Ghane, N. and Sadrnezhaad, S.K. (2020) Combustion synthesis of g-C_3N_4/Fe_2O_3 nanocomposite for superior photoelectrochemical catalytic performance. *Appl. Surf. Sci.*, *534*, 147563.
- Ghasemi, F. and Amiri, M.H. (2021) Facile in situ fabrication of rGO/MoS_2 heterostructure decorated with gold nanoparticles with enhanced photoelectrochemical performance. *Appl. Surf. Sci.*, *570*, 151228.
- Goettmann, F., Fischer, A., Antonietti, M., & Thomas, A. (2006) Chemical Synthesis of Mesoporous Carbon Nitrides Using Hard Templates and Their Use as a Metal-Free Catalyst for Friedel–Crafts Reaction of Benzene. Angew. Chem. Int. Ed., 45(27), 4467-4471.
- Guigoz, V., Balan, L., Aboulaich, A., Schneider, R. and Gries, T. (2020) Heterostructured thin $LaFeO_3$/g-C_3N_4 films for efficient photoelectrochemical hydrogen evolution. *Int. J. Hydrog. Energy*, *45*(35), 17468-17479.
- Guru, S. (2021) Bismuth oxycarbonate grafted NiFe-LDH supported on g-C_3N_4 as bifunctional catalyst for photoelectrochemical water splitting. *Int. J. Hydrog. Energy*, *46*(22), 12145-12157.
- Kawrani, S., Boulos, M., Bekheet, M.F., Viter, R., Nada, A.A., Riedel, W., Roualdes, S., Cornu, D. and Bechelany, M. (2020) Segregation of copper oxide on calcium copper titanate surface induced by Graphene Oxide for Water splitting applications. *Appl. Surf. Sci.*, *516*, 146051.
- Kim, T.G., Samuel, E., Park, C.W., Joshi, B., Kim, M.W., Swihart, M.T. and Yoon, S.S. (2020) Supersonically sprayed Zn_2SnO_4/SnO_2/carbon nanotube films for high-efficiency water splitting

photoanodes. *J. Alloys Compd.*, *828*, 154374.

- Li, S., Jiang, Y., Jiang, W., Zhang, Y., Pan, K., Wang, S., Hu, C., Zhang, L.H. and Xia, L. (2020) In-situ generation of g-C_3N_4 on $BiVO_4$ photoanode for highly efficient photoelectrochemical water oxidation. *Appl. Surf. Sci.*, *523*, 146441.
- Liao, F., Shi, Y., Dang, Q., Yang, H., Huang, H., Kang, Z. and Shao, M. (2022) Carbon dots dominated photoelectric surface in titanium dioxide nanotube/nitrogen-doped carbon dot/gold nanocomposites for improved photoelectrochemical water splitting. *J. Colloid Interface Sci.*, *606*, 1274-1283.
- Moakhar, R.S., Soleimani, F., Sadrnezhaad, S.K., Masudy-Panah, S., Katal, R., Seza, A., Ghane, N. and Ramakrishna, S. (2020) One-pot microwave synthesis of hierarchical C-doped CuO dandelions/g-C_3N_4 nanocomposite with enhanced photostability for photoelectrochemical water splitting. *Appl. Surf. Sci.*, *530*, 147271.
- Mohamed, N.A., Ismail, A.F., Safaei, J., Johan, M.R. and Teridi, M.A.M. (2021) A novel photoanode based on Thorium oxide (ThO_2) incorporated with graphitic Carbon nitride (g-C_3N_4) for Photoelectrochemical water splitting. *Appl. Surf. Sci.*, *569*, 151043.
- Reddy, A.S. and Kim, J. (2020) An efficient g-C_3N_4-decorated CdS-nanoparticle-doped Fe_3O_4 hybrid catalyst for an enhanced H_2 evolution through photoelectrochemical water splitting. *Appl. Surf. Sci.*, *513*, 145836.
- Reddy, I.N., Reddy, L.V., Jayashree, N., Reddy, C.V., Cho, M., Kim, D. and Shim, J. (2021) Vanadium-doped graphitic carbon nitride for multifunctional applications: Photoelectrochemical water splitting and antibacterial activities. *Chemosphere*, *264*, 128593.
- Reddy, I.N., Sreedhar, A., Manjunath, V., Shim, J. and Noh, J.S. (2021) Water splitting kinetics of Sr-doped g-C_3N_4 edge-wrinkled nanosheets under visible light. *Mater Sci Semicond Process*., *132*, 105918.
- Sajjadizadeh, H.S., Goharshadi, E.K. and Ahmadzadeh, H. (2020). Photoelectrochemical water splitting by engineered multilayer TiO_2/GQDs photoanode with cascade charge transfer structure. *Int. J. Hydrog. Energy*, *45*(1), 123-134.

- Seo, Y.J., Das, P.K., Arunachalam, M., Ahn, K.S., Ha, J.S. and Kang, S.H. (2020) Drawing the distinguished graphite carbon nitride (g-C_3N_4) on SnO_2 nanoflake film for solar water oxidation. *Int. J. Hydrog. Energy*, *45*(43), 22567-22575.
- Sharma, D., Yadav, J. and Mehta, B.R. (2021) Reduced graphene oxide layer on nanostructured SnS thin films for improved visible light photoelectrochemical activity. *Renew. Energy*, *169*, 414-424.
- Sial, Q.A., Singh, R., Iqbal, S., Yoo, I.H., Kalanur, S.S. and Seo, H. (2021) Nitrogen-doped carbon dot anchored 1-D WO_3 for enhanced solar water splitting: A nano surface imaging evidence of charge separation and accumulation *Int. J. Hydrog. Energy*, *46*(64), 32546-32558.
- Tang, X., Guo, X., Chen, Z., Liu, Y., Zhang, W., Wang, Y., Zheng, Y., Zhang, M., Peng, Z., Li, R. and Zhao, Y. (2020) Facile preparation of Cu_2O nanoparticles/Bi_2WO_6/rGO hybrid with enhanced photoelectrochemical performance. *Appl. Surf. Sci.*, *510*, 145447.
- Wang, L., Cai, P., Liu, Z., Xie, Z. and Fang, Y. (2022) Role of carbon quantum dots on Nickel titanate to promote water oxidation reaction under visible light illumination. *J. Colloid Interface Sci.*, *607*, 203-209.
- Xiao, C., Lei, B., Jin, W. and Xu, L. (2021) Candle flame fabrication of carbon coated CuO-Cu_2O composite photocathode for photoelectrochemical water reduction. *Mater. Lett.*, *298*, 130006.
- Yaw, C.S., Ng, W.C., Ruan, Q., Tang, J., Soh, A.K. and Chong, M.N. (2020) Tuning of reduced graphene oxide thin film as an efficient electron conductive interlayer in a proven heterojunction photoanode for solar-driven photoelectrochemical water splitting. *J Alloys Compd.*, *817*, 152721.
- Zargazi, M. and Entezari, M.H. (2021). Photoelectrochemical water splitting by a novel design of photo-anode: inverse opal-like UiO-66 sensitized by Pd and decorated with S, N graphene QDs. *Electrochim. Acta*, *391*, 138926.
- Zhang, X., Bian, X., Xu, H. and Wu, W. (2021). Fabrication of WO_3/RGO/Ni: FeOOH heterostructure for synergistically enhancing photoelectrochemical water oxidation. *Appl. Surf. Sci.*, *542*, 148579.
- Zhao, J., Liu, C.A., Wang, H., Fu, Y., Zhu, C., Huang, H., Liao, F., Liu, Y., Shao, M. and Kang,

Z. (2020) Carbon dots modified WO_2-Na_xWO_3 composite as UV-Vis-NIR broad spectrum-driven photocatalyst for overall water splitting. *Catal. Today*, *340*, 152-160.

- Zhou, T., Chen, S., Li, L., Wang, J., Zhang, Y., Li, J., Bai, J., Xia, L., Xu, Q., Rahim, M. and Zhou, B. (2020) Carbon quantum dots modified anatase/rutile TiO_2 photoanode with dramatically enhanced photoelectrochemical performance. *Appl. Catal. B.*, *269*, 118776.